ELSEVIER

Finite Elements in Analysis and Design 16 (1994) 337–348

FINITE ELEMENTS IN ANALYSIS AND DESIGN

Spectral element method for acoustic wave simulation in heterogeneous media

Géza Seriani*, Enrico Priolo

Osservatorio Geofisico Sperimentale, P.O. Box 2011, 34016 Trieste, Italy

Abstract

In this paper, we present a spectral element method for studying acoustic wave propagation in complex geological structures. Due to complexity (both lithological and stratigraphical), the use of numerical methods of higher accuracy and flexibility is needed to achieve the correct results. The spectral element method shows more accurate results compared to the low-order finite element, the conventional finite difference and the pseudospectral methods. High accuracy is reached even for rather long wave propagation times and dispersion errors are essentially eliminated; pirregular interfaces between different media can be well described so that numerical artifacts or noises are not at all introduced. The method is tested against analytical solutions both in the two-dimensional homogeneous and heterogeneous media. The results of different simulations are presented.

1. Introduction

Seismic forward modeling is a valuable tool for studying wave propagation in complex geological structures. The most widespread of the discrete numerical methods for modeling seismic wave propagation is the finite difference (FDM) the Fourier or pseudospectral (PSM) and the finite element (FEM) methods [1,2]. All three methods rely on the space discretization of the geological structure to be modeled. In particular, the pseudospectral method can be seen as a limiting case of the finite difference methods of increasing order and accuracy [2]. The main advantage of the PSM is its great accuracy, as it allows for a lower number of grid points per minimum wave-length propagating in the model and therefore help to save up to several orders of magnitude in computer memory and time. On the other hand, the FEM is well-known for its flexibility in describing problems with complex geometries: irregular surfaces between different media can be defined with great accuracy. The use of the spectral element method (SPEM) which combines PSM accuracy with FEM flexibility is highly desirable for seismic wave modeling. SPEM was introduced by

*Corresponding author.

0168-874X/94/$07.00
SSDI 0168-874X(93)E0103-8

Patera and co-workers, and its accuracy and efficiency are demonstrated in [3,4]. Various authors have further developed this method mainly for fluid dynamic problems.

The spectral element method is based on the idea of decomposing the original domain into non overlapping quadrilateral elements and then, in the case of acoustic problems, the pressure field at each time step is computed, ensuring that the variational statement is satisfied for the piecewise-polynomial space where the field is approximated. The approximation space is built using a tensor product of orthogonal functions. The authors have investigated the accuracy of the method for wave propogation by analyzing the results of a set of numerical experiments [5,6]. The main conclusion is that a low value of G (the number of grid points per minimum wavelength), is needed to correctly propagate an impulse during a numerical simulation and that the accuracy is almost unchanged even for very long propagation times. Using the method, one can see that the dispersion errors were essentially eliminated. A value of $G = 4.5$, for example, is needed for a correct wave propagation by using polynomials of order $N = 8$ compared with the values of $G = 15$–30 which are needed when using low order finite difference or finite element schemes.

In the case of a very coarse grid (which is sufficient to propagate an impulse in the pseudospectral method), because of the interfaces between different media which appear jagged to the rectangular grid large inavoidable errors are caused [7]. The roughness in the discretization of a smooth interface not aligned with the grid acts as a source of non-physical noise that in many cases can hide subtle but interesting physical phenomena. Even worse, if many interfaces are present, very noisy multiple reflections and transmission events will be produced. From this point of view, SPEM is far superior to pseudospectral or other rectangular fixed grid methods, since interfaces can be aligned with the grid and the interface noise can be eliminated.

In the present work, the spectral element method for acoustic wave propagation in heterogeneous media is presented. The accuracy and convergence properties for wave propagation in homogeneous media are reviewed and then the numerical results for simulation in heterogeneous media and the interface representation problem are discussed. Simulation for a typical geological structure is then discussed.

2. Mathematical formulation

2.1. Two-dimensional acoustic wave equation

In a bounded, inhomogeneous medium the acoustic dilatation (pressure) is described by the governing equation;

$$\frac{\partial}{\partial t^2}\left(\frac{1}{\rho c^2}\frac{\partial u}{\partial t}\right) - \nabla\cdot\left(\frac{1}{\rho}\nabla u\right) = f \quad \text{in } \Omega\times[0, T] \tag{1}$$

with some suitable conditions specified on the boundaries and some prescribed initial conditions for the acoustic field. In (1), $u(x, y, t)$ is the pressure field, $\rho(x, y)$ is the density, $c(x, y)$ is the wave velocity and $f(x, y, t)$ is the source forcing term which equals the divergence of the body force divided by the density. We denote by t the time variable defined over the interval $[0, T]$, and Ω the physical domain.

If we look for sufficiently regular solutions u, an equivalent, variational formulation of equation (1) is to find $u(x, y, t) \in H_0^1(\Omega) \times [0, T]$ solution of

$$\frac{d^2}{dt^2} \int_\Omega w \frac{1}{\rho c^2} u \, d\Omega + \int_\Omega \nabla w \cdot \left(\frac{1}{\rho} \nabla u \right) d\Omega = \int_\Omega w f \, d\Omega \quad \forall w \in H_0^1(\Omega), \tag{2}$$

where H_0^1 is the space of all functions which vanish on the boundaries and which, together with their first derivatives, are square integrable over Ω. In equation (2), perfect reflecting boundary conditions are implied, this means that when the acoustic wave reaches the boundary of Ω, it reflects back interfering with the outgoing waves. In many physical problems, like in geophysics, wave propagation must be simulated in an unbounded spatial domain using a finite domain due to the restriction of computer resources. In that case, for a numerical simulation an artificial boundary treatment is introduced which either absorbs the acoustic energy or is nonreflecting. In the first case, an absorbing strip is added outside the boundary enlarging de facto the computational domain. In such a strip the acoustic energy is smoothly attenuated by using a damping mechanism. In the second case, a mathematical nonreflecting boundary condition (NRBC) is applied at the boundary of the computational domain Ω. A variety of NRBC have been analyzed by many authors. Here we consider a modified second order paraxial approximation to take into account the effects of the boundary curvatures [8, 9]. The condition is given by

$$\frac{1}{\rho c} \frac{\partial^2 u}{\partial t^2} + \frac{1}{\rho} \frac{\partial^2 u}{\partial t \, \partial n} + \frac{\kappa}{2} \frac{\partial u}{\partial t} - \frac{c}{2\rho} \frac{\partial^2 u}{\partial \tau^2} = 0 \quad \text{on } \Gamma \tag{3}$$

where κ is the curvature on the boundary Γ of the domain, $\partial u / \partial n$ and $\partial u / \partial \tau$ are the normal and tangential derivative on Γ respectively. Coupling the boundary condition (3) to the governing equation (1), the equivalent variational formulation is then expressed as to find $u(x, y, t) \in H^1(\Omega) \times [0, T]$ subject to:

$$\frac{d^2}{dt^2} \int_\Omega w \frac{1}{\rho c^2} u \, d\Omega + \frac{d}{dt} \int_\Gamma w \frac{1}{\rho c} u \, d\Gamma + \int_\Omega \nabla w \cdot \left(\frac{1}{\rho} \nabla u \right) d\Omega + \frac{1}{2} \int_\Gamma w \frac{\kappa}{\rho} u \, d\Gamma$$
$$+ \frac{1}{2} \int_0^T \int_\Gamma \frac{c}{\rho} \frac{\partial w}{\partial \tau} \frac{\partial u}{\partial \tau} \, d\Gamma \, dt = \int_\Omega w f \, d\Omega \quad \forall w \in H_0^1(\Omega). \tag{4}$$

Note that three more terms emerge now in the variational equation, coming from the boundary condition (3). From a computational point of view, the time integration of the fifth term can be performed using a trapezoidal rule where the whole integral is not computed at each time step, but an intermediate value is stored and then updated.

2.2. Spectral element approximation

In order to obtain the spectral-element approximation of the equation (2) or (4), we decompose $\bar{\Omega}$ into rectangular nonoverlapping elements Ω_e, where $e = 1, \ldots, n_e$ and n_e is the total number of elements, and then we require that the variational statement be satisfied for the acoustic wave field approximating space build up as a sum of elemental approximating functions. In each element Ω_e, we choose the approximating functions from the $\mathbb{P}_{N_x} \otimes \mathbb{P}_{N_y}$ space i.e., the tensor product space of all

polynomials of degree $\leqslant N_x$ in x and of degree $\leqslant N_y$ in y. If the physical domain is not rectangular or has an internal structure which is not regular, it is not possible to make a decomposition by using rectilinear elements. In this case, a spatial discretization with general (non-rectilinear, or curved) quadrilateral elements must be used. The computation of the elemental integrals for such curvilinear elements Ω_e would be awkward if performed directly. It can be simplified by introducing an invertible transformation between a *reference* or *master* element $\hat{\Omega}$, where all computations will take place, and the general element Ω_e. In our case, the reference element is defined to be the square interval $\hat{\Omega} = [-1, 1] \times [-1, 1]$. Using an interpolant Chebyshev Gauss Lobatto basis, the spectral element approximation in $\hat{\Omega}$ for a function $f(x, y)$ is defined as follows:

$$\tilde{f}(x, y) = \sum_{i=0}^{N} \sum_{j=0}^{N} \tilde{f}_{ij} \varphi_i(x) \varphi_j(y), \tag{5}$$

where $\tilde{f}_{ij} = f(x_i, y_j)$ are the grid values of the function f and $\varphi_i(\zeta) \in \mathbb{P}_N$ are the Lagrangian interpolants satisfying the relation $\varphi_i(\zeta_k) = \delta_{ik}$ within the interval $[-1, 1]$ and identically zero outside. Here δ_{ik} denotes the Kronecker-delta symbol and ζ stands for x or y. The Lagrangian interpolants are given by,

$$\varphi_i(\zeta) = \frac{2}{N} \sum_{p=0}^{N} \frac{1}{\bar{c}_i \bar{c}_p} T_p(\zeta_i) T_p(\zeta), \quad \bar{c}_i = \begin{cases} 1 & \text{for } i \neq 0, N, \\ 2 & \text{for } i = 0, N, \end{cases} \tag{6}$$

where T_p are the Chebyshev polynomials and ζ_i, are the Chebyshev–Gauss Lobatto quadrature points $\zeta_i = \cos(\pi i / N)$ for $i = 0, \ldots, N$. The coordinates of the internal nodes in the quadrilateral domain $\hat{\Omega}$ are obtained as Cartesian products of the ζ_i points. The mapping between $\hat{\Omega}$ and Ω_e is of isoparametric type and is defined, using a tensorial product, according to

$$\{x, y\}_N^e = \sum_{i=0}^{N} \sum_{j=0}^{N} \{x^*, y^*\}_{ij}^e \varphi_i(\xi) \varphi_j(\eta), \tag{7}$$

where $\{x^*, y^*\}_{ij}^e$ are the physical coordinates $\{x, y\}$ in the element Ω_e of the grid point mapped to $\{\xi_i, \eta_j\}$ in $\hat{\Omega}$.

To solve the variational problem on the decomposition of $\bar{\Omega}$ we define the trial functions $\tilde{u}(x, y, t)$ and the weight functions $\tilde{w}(x, y)$ such that

$$\tilde{u}(x, y, t) = \bigcup_{e=1}^{n_e} \tilde{u}_e(x, y, t), \qquad \tilde{w}(x, y) = \bigcup_{e=1}^{n_e} \tilde{w}_e(x, y), \tag{8}$$

where $\tilde{u}_e$ and $\tilde{w}_e$ denote the restriction to Ω_e of $\tilde{u}$ and $\tilde{w}$, respectively. The equivalent finite-dimensional spaces are given by

$$S_N = \{\tilde{u}(x, y, t) \in C^0(\bar{\Omega} \times [0, T]) \mid \tilde{u}_e \in \mathbb{P}_{N_e}; \text{ for } e = 1, \ldots, n_e; \tilde{u}(\cdot, t) = 0 \text{ on } \Gamma\},$$

for the trial functions and

$$V_N = \{\tilde{w}(x, y) \in C^0(\bar{\Omega}) \mid \tilde{w}_e \in \mathbb{P}_{N_e}, \text{ for } e = 1, \ldots, n_e, \quad \tilde{w}(\cdot) = 0 \text{ on } \Gamma\},$$

for the weight functions, where n_e is total number of subdomains. Here N_e, denotes the pair (N_x^e, N_y^e), and $\mathbb{P}_{N_e}$ is defined to be $\mathbb{P}_{N_x^e} \otimes \mathbb{P}_{N_y^e}$. The functions $\tilde{u}_e$ and $\tilde{w}_e$, are given by an expansion

similar to equation (5) where $\tilde{u}_{ij}^{(e)}(t) = \tilde{u}_e(x_i^{(e)}, y_j^{(e)}, t)$ and $\tilde{w}_{ij}^{(e)} = \tilde{w}_e(x_i^{(e)}, y_j^{(e)})$, i.e. the grid values for the unknown approximate solution and for the weight functions respectively, are used instead of $\tilde{f}_{ij}$. Using these definitions, it follows that the two dimensional wave propagation problem is equivalent to finding $\tilde{u}_e$ such that for all $\tilde{w}_e$ the following equation is satisfied over $\bar{\Omega}$:

$$\sum_{e=1}^{n_e} \left\{ \frac{\mathrm{d}^2}{\mathrm{d}t^2} \int_{\hat{\Omega}} |J^{(e)}| \tilde{w}_e \frac{1}{\rho c^2} \tilde{u}_e \,\mathrm{d}\xi \,\mathrm{d}\eta + \frac{\mathrm{d}}{\mathrm{d}t} \int_{-1}^{+1} |J_S^{(e)}| \tilde{w}_e \frac{1}{\rho c} \tilde{u}_e \,\mathrm{d}\xi \right.$$
$$+ \int_{\hat{\Omega}} \frac{1}{|J^{(e)}|} \hat{\nabla} \tilde{w}_e \cdot \left(\frac{1}{\rho} \hat{\nabla} \tilde{u}_e \right) \mathrm{d}\xi \,\mathrm{d}\eta + \frac{1}{2} \int_{-1}^{+1} |J_S^{(e)}| \tilde{w}_e \frac{\kappa}{\rho} \tilde{u}_e \,\mathrm{d}\xi$$
$$\left. + \frac{1}{2} \int_0^T \int_{-1}^{+1} \frac{1}{|J_S^{(e)}|} \frac{c}{\rho} \frac{\partial \tilde{w}_e}{\partial \zeta} \frac{\partial \tilde{u}_e}{\partial \zeta} \mathrm{d}\zeta \,\mathrm{d}t \right\} = \sum_{e=1}^{n_e} \left\{ \int_{\hat{\Omega}} |J^{(e)}| \tilde{w}_e \tilde{f}_e \,\mathrm{d}\xi \,\mathrm{d}\eta \right\}, \quad \forall \tilde{w}_e \in \mathbb{P}_{N_e}(\Omega_e), \tag{9}$$

where (ξ, η) are the local coordinates in $\hat{\Omega}$, and ζ is the arc-length coordinate in elements which have a side on the boundary of the domain Ω where boundary conditions are prescribed. The function $|J^{(e)}|$ is the Jacobian of the transformation from global to local coordinates and $|J_S^{(e)}|$ is the Jacobian of the transformation for the arc-length on the boundary. The operator $\hat{\nabla}$ is given by

$$\hat{\nabla} = \left\{ \frac{\partial y}{\partial \eta} \frac{\partial}{\partial \xi} - \frac{\partial y}{\partial \xi} \frac{\partial}{\partial \eta}, \; - \frac{\partial x}{\partial \eta} \frac{\partial}{\partial \xi} + \frac{\partial x}{\partial \xi} \frac{\partial}{\partial \eta} \right\}. \tag{10}$$

Using the previous definition (6) and $\varphi_i(\zeta)$, we can compute the derivative matrix $D_{ij} = \mathrm{d}\varphi_i(\zeta_i)/\mathrm{d}\zeta$ and the geometric transformation factors according to

$$\left(\frac{\partial \{x, y\}}{\partial \xi} \right)_{ij}^e = \sum_{k=0}^{N} \{x^*, y^*\}_{kj}^e D_{ki}, \qquad \left(\frac{\partial \{x, y\}}{\partial \eta} \right)_{ij}^e = \sum_{k=0}^{N} \{x^*, y^*\}_{ik}^e D_{kj}. \tag{11}$$

Then the two Jacobians and the operator $\hat{\nabla}$ can be evaluated easily at each collocation point, in the same fashion we procede to compute the curvature κ and the derivatives with respect to the arc-length coordinate ζ. Finally we evaluate the elemental integrals and requiring that the variational equation be satisfied for all $\tilde{w}_e$, the spectral element approximation of our original equation leads to solve a set of linear equations;

$$\boldsymbol{M}\{\ddot{\boldsymbol{U}}\} + \boldsymbol{C}\{\dot{\boldsymbol{U}}\} + \boldsymbol{K}\{\boldsymbol{U}\} + \int_0^T \boldsymbol{B}\{\boldsymbol{U}\} \,\mathrm{d}t = \{\boldsymbol{F}\}, \tag{12}$$

with $\{\boldsymbol{U}(0)\} = \{\boldsymbol{U}_0\}$, $\{\dot{\boldsymbol{U}}(0)\} = \{\dot{\boldsymbol{U}}_0\}$ as initial conditions, where the unknown vector $\{\boldsymbol{U}\}$ contains the values of the discrete solution $\tilde{u}$ at all collocation points and where $\boldsymbol{M}$ is the mass matrix, $\boldsymbol{K}$ is the stiffness matrix, and $\{\boldsymbol{F}\}$ is the force vector. The matrices $\boldsymbol{C}$ and $\boldsymbol{B}$ take into account the effect of the nonreflecting boundary condition, they are null matrices if this condition is not used. All the matrices are global matrices built up by direct stiffness summation of the corresponding elemental matrices to enforce the continuity requirement of the solution on the element boundaries. To solve the system of linear equations (12) we must integrate over the time interval $[0, T]$. This may be done by discretizing the time variable as $t_n = n\Delta t$, $0 \leqslant n \leqslant N_T$, where $\Delta t = T/N_T$, and N_T is the total number of time steps. The solution at time t_n, is $\{\boldsymbol{U}_n\} = \{\boldsymbol{U}(t_n)\}$. As time integration scheme, we use the Newmark constant average acceleration scheme, which is a two-step implicit algorithm, unconditionally stable and second-order accurate [10]. When

matrices $\boldsymbol{C}$ and $\boldsymbol{B}$ vanish, the Newmark method is quite straightforward to implement. In the opposite case some modifications are required. In particular the effect of fourth term in equation (12) is computed by considering its contribution as a fictitious force updated at each time step. The solution at time t_{n+1} is obtained by solving a sparse, symmetric system of linear equations of the form $A\{\boldsymbol{U}_{n+1}\} = \{b_n\}$. Due to overall computational efficiency considerations, the system is solved by using a preconditioned conjugated gradient method.

3. Accuracy analysis

A numerical accuracy analysis of the method was presented in [5] for the 1D case. For large scale modeling, it is important that the accuracy is stable in time; the rate of the accuracy decay during the propagation was determined in [5] for a large number of polynomial orders. A similar analysis, even if less extensive, was then performed for the 2D case. As expected, the same results were obtained, since the 2D formulation was achieved by a tensor product of the 1D interpolation base.

The starting point of this study was that numerical modeling for wave propagation actually behaves as a low-pass filter, in the sense that low frequencies accurately propagate through the mesh whereas high frequencies are undesirably modified [1]. The most evident numerical effects (in the high-frequency band) are numerical attenuation, numerical anisotropy, dispersion in numerical phase and group velocity, and numerical polarization. Due to this fact, frequency analysis is a very suitable approach for the investigation of numerical modeling results. It makes it easier to determine the spectral band in which the equation is solved correctly; that is to find the minimum wavelength for which a given numerical method is accurate. The *frequency error-index*, a complex function defined as $\boldsymbol{H}(\omega) = \boldsymbol{U}_{\text{num}}(\omega)/\boldsymbol{U}_{\text{an}}(\omega) = |\boldsymbol{H}(\omega)|\,e^{i\phi(\omega)}$, where $\boldsymbol{U}_{\text{an}}(\omega)$ and $\boldsymbol{U}_{\text{num}}(\omega)$ are the Fourier transforms of the analytical and numerical solutions which we want to compare, was then introduced. The frequency error-index makes the interpretation of the results effective since it is not affected by the spectrum of the chosen initial impulse but depends only on the numerical model. By considering both the real and the imaginary part of the frequency error-index, the decrease of accuracy due to the amplitude variations (when $|\boldsymbol{H}(\omega)| \neq 1$) and the velocity dispersion (when $\phi = \text{arctg}(\text{Im}\{\boldsymbol{H}(\omega)\}/\text{Re}\{\boldsymbol{H}(\omega)\}) \neq 0$) can be analyzed.

A broad-band pulse was propagated for the long distances, and for each order of approximation, it was possible to identify (see Fig. 1) a low-frequency band where the analytical and the numerical solutions agree ($|\boldsymbol{H}(\omega)| = 1$ and $\phi = 0$). The maximum extreme of this interval corresponds to the minimum number of grid points per wavelength, $G_{\min}(N)$, for which the solution is good. The minimum wavelength that the model can propagate without appreciable errors is then $\lambda_{\min}(N) = G_{\min}(N)\Delta x$.

The main conclusions, as inferred from Fig. 2, can be summarized as follows. A low value of G (the number of grid points per minimum wavelength), is needed to correctly propagate an impulse during a numerical simulation, and great accuracy is obtained for the propagation of waves whose spectrum lies below the wavelength corresponding to the correct $G_{\min}(N)$. Moreover, the theoretical limit of $G = \pi$ is asymptotically reached for increasing orders. The accuracy remains almost unchanged even for very long propagation times. Dispersive errors are essentially eliminated. An almost constant value of $G \approx 4.5$, for example, is needed for a correct wave

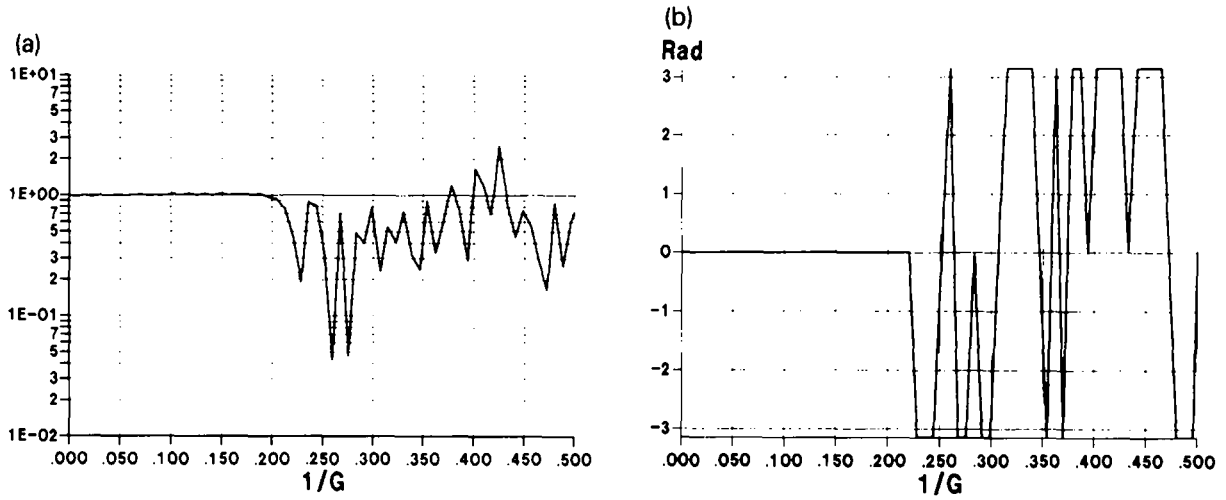

Fig. 1. Amplitude (a) and phase (b) of the frequency error-index for 1D SPEM with polynomial order $N = 8$ after 960 grid-points of propagation.

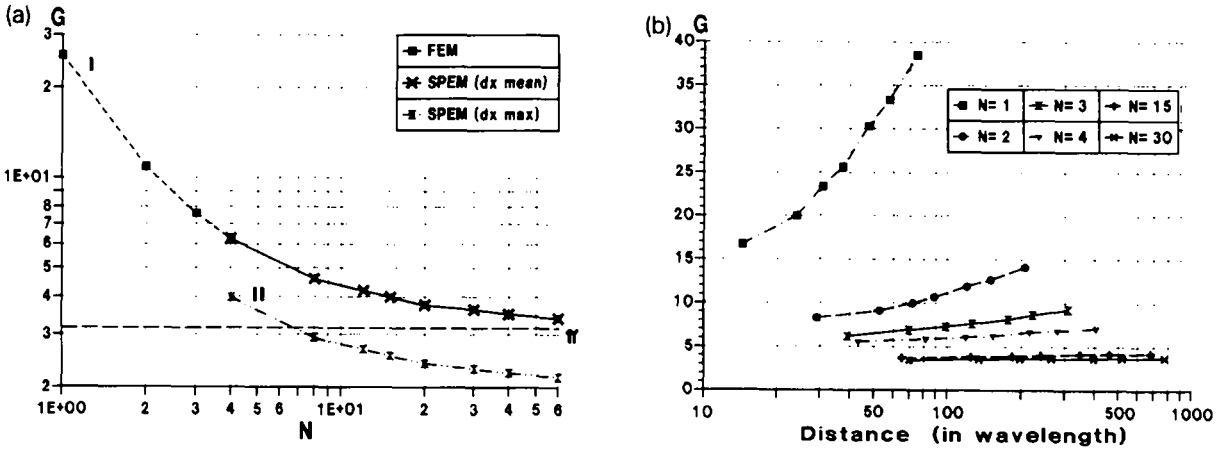

Fig. 2. G_{min} values versus polynomial order (a) and travel distance (b), respectively.

propagation by using polynomials of order $N = 8$ compared with the rapidly increasing values of $G \approx 15$ 30 that are needed when using low-order finite difference or finite element schemes.

Accuracy is usually considered for wave propagation in homogeneous media. In inhomogeneous media, the accuracy can be reduced. The reliability of the method is now demonstrated on an inhomogeneous model, the wedge model, for which an analytical solution is available [11]. The analytic solution computes the scattered field of a plane acoustic waves impinging on a wedge of arbitrary angle with different constant velocities inside and outside the wedge. The geometry and the velocity used for the numerical model are described in Fig. 3(a). Fig. 3(b) shows the comparison between the analytical and SPEM solutions of the scattered pressure field computed in R. A horizontal Ricker plane wave was impinging on the wedge from above. The Ricker wave has

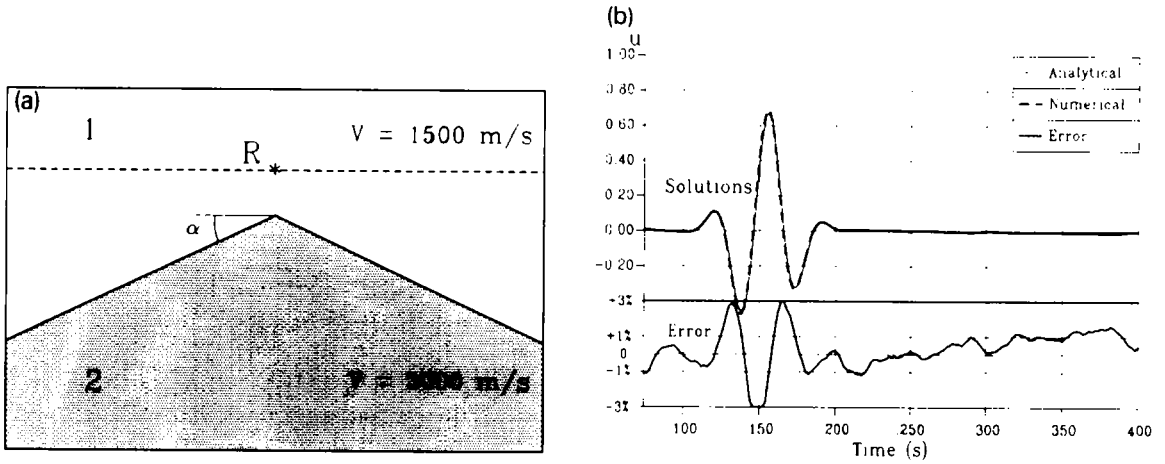

Fig. 3. The wedge model. (a) Description of the model. The angle of the wedge with the horizontal is $\alpha = \text{arctg}(0.5) \approx 26.5$. (b) Comparison between the analytical and numerical solutions collected at point R. The two time histories (upper curves) and the error (lower curve) are shown.

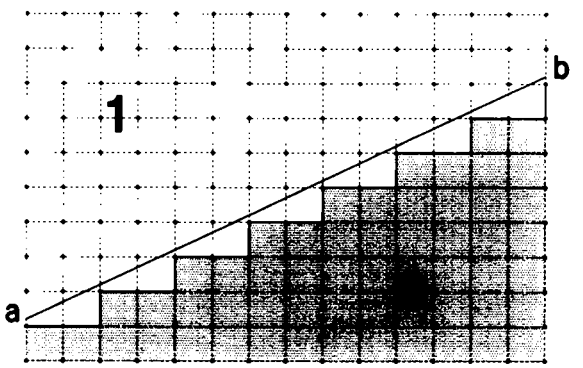

Fig. 4. An inclined interface (solid line connecting a to b) jagged to the rectangular grid.

a central frequency of 27 Hz and a cut-off frequency of 55 Hz. A polynomial order $N = 8$ was taken for SPEM, corresponding to $G \approx 4.5$. The numerical and analytical results match very well and the maximum absolute error is contained below the 3%, even by using single precision floating point arithmetic.

4. The interface representation problem

It was pointed out that the pseudospectral method is the most accurate for wave propagation in a homogeneous medium. Anyway, when using a very coarse grid ($G \approx 2$) which is sufficient to propagate an impulse using this method, the interfaces between different structures appear jagged to the rectangular grid (see Fig. 4). This leads to large errors which are unavoidable [7]. The roughness in the discretization of a smooth interface not aligned with the grid acts as a source of

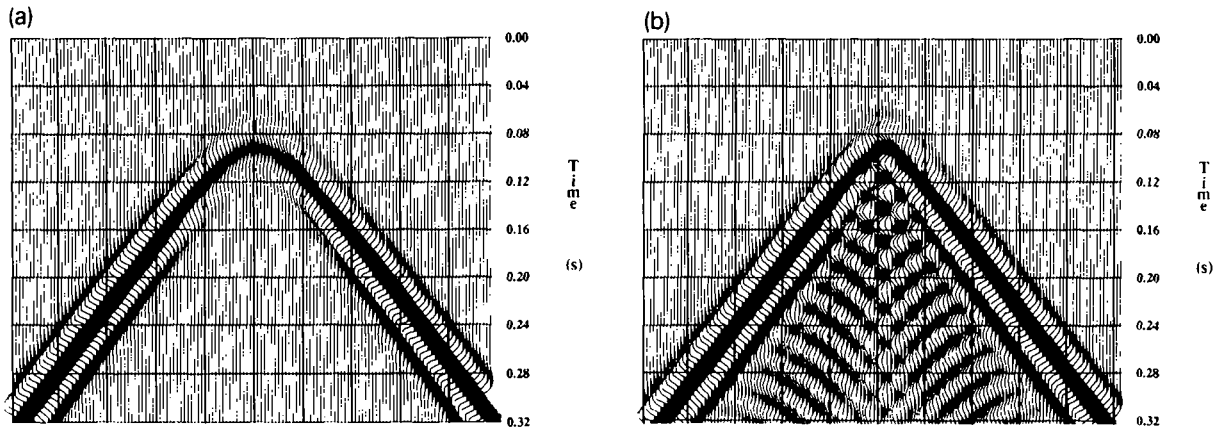

Fig. 5. Time histories of the wedge collected at the dashed line of Fig. 3(a) and computed using the SPEM (a), and the PSM (b), respectively.

nonphysical noise that in many cases can hide subtle but interesting physical phenomena. Even worse, if many interfaces are present, very noisy multiple reflections and transmission events will be produced.

From this point of view, the SPEM is far superior to pseudospectral or other rectangular fixed grid methods since the interfaces can be aligned with the grid and the interface noise can be eliminated. Moreover, curved interfaces coming out from SPEM discretization correspond to the interpolation obtained by using the high-order polynomials defined over the elements. The resulting modeled interface does not contain vertices or cusps arising from a bad reconstruction, which can give rise to diffractions.

The numerical effects of two different configurations of inclined interfaces when using both SPEM and Fourier pseudospectral methods (PSM) are illustrated here. In the first experiment the same wedge model of the preceding section was used and solved by PSM. A grid size corresponding to $G \approx 2$ was taken. Fig. 5 shows the time histories computed with the two methods collected along a horizontal line above the wedge (the dashed line in Fig. 3(a)). The results obtained by PSM (Fig. 5(b)) clearly show the patterns corresponding to the diffracted waves arising from the poor reconstruction of the interface.

In the second experiment the response of a wedge-shaped layer was simulated again by both SPEM and PSM. The geometry and the physical parameters of the model are shown in Fig. 6. Fig. 7(b) depicts the time histories collected along the horizontal line above the layer (the dashed line in Fig. 6) obtained using the SPEM (Fig. 7(a)) and the PSM (Fig. 7(b)), respectively. The effect of having just a layer instead of the whole half-space is clearly seen by comparing two sets of time histories computed using the SPEM (Figs. 5(a) and 7(a)). The synthetic seismograms corresponding to the PSM simulation (using $G = 2$) can be seen in Figs. 5(b) and 7(b) respectively. They are undistinguishable from those obtained from the simple wedge model, so that all information arising from the layer is definitely lost. To obtain the same accuracy of the SPEM, a value $G \approx 5$ must be used with PSM. To model complex geological configurations, as for example for stratigraphic structures characterized by thin layers, an even greater value of G is needed, so loosing the efficiency of PSM.

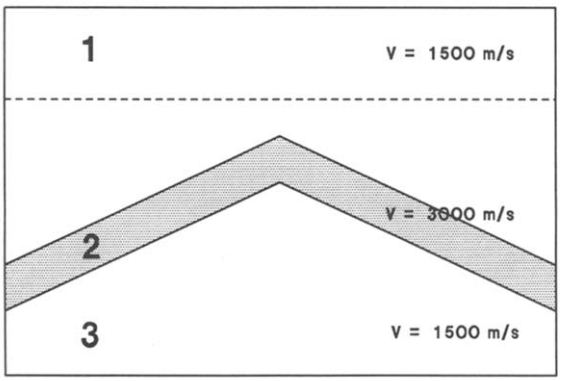

Fig. 6. The wedge-shaped layer model. The normal thickness of the layer is 73 m. The inclination is the same as for the simple wedge.

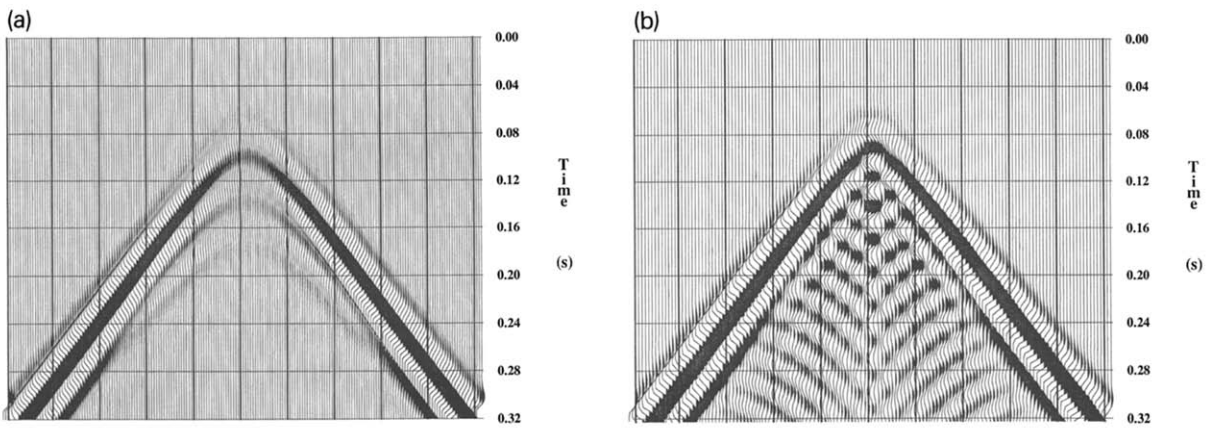

Fig. 7. Time histories of the wedge-shaped layer collected at the dashed line of Fig. 6 and computed using the SPEM (a), and the PSM (b), respectively.

5. A numerical example

A more realistic situation is shown on an example of an inclined stratified fault. The geometry and the physical parameters are given in Fig. 8(a). Free boundary conditions are imposed at the surface. The source is a vertical point source (indicated by a star) applied at the surface. Chebyshev spectral elements of order 8 ($G \approx 4.5$) were used. Figs. 8(a) to 8(d) show snapshots of the pressure field at propagation times 0.11 s, 0.23 s, 0.35 s and 0.47 s, respectively. No diffracted waves due to the inclined interface can be observed. A guided wave effect can be seen in the top layer.

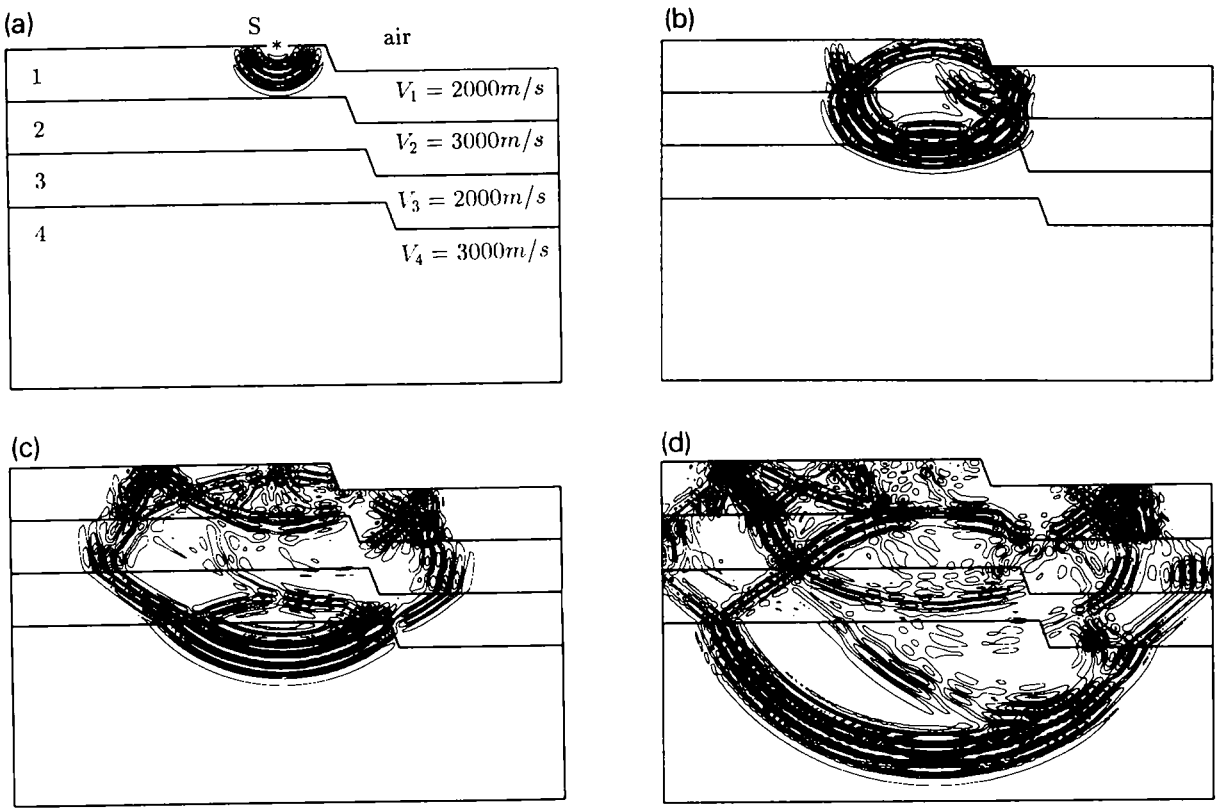

Fig. 8. Acoustic wave propagation in an inclined stratified fault due to a point source. A free surface condition is imposed at the top.

Acknowledgements

This research was supported in part by the Commission of the European Communities under the JOULE programme (1989–1992), Sub-programme: Hydrocarbons. The authors wish to express special thanks to P. Berg, F. If, P. Nielsen and O. Skoovgard of the Laboratory of Applied Mathematical Physics at the Technical University of Denmark who kindly provided us with an analytic solution to the wedge problem.

References

[1] K.J. Marfurt, "Accuracy of finite-difference and finite-element modelling of the scalar and elastic wave equations", *Geophys.* **49**, pp. 535–549, 1984.

[2] B. Fornberg, "The pseudospectral method: Comparisons with finite differences for the elastic wave equations", *Geophys.* **52**, pp. 483–501, 1987.

[3] A.T. Patera, A spectral element method for fluid dynamics: Laminar flow in a channel expansion", *J. Comp. Phys.* **54**, pp. 468–488, 1984.

[4] Y. Maday and A.T. Patera, "A spectral element method for the incompressible Navier Stokes Equations", in: A.K. Noor (ed.), *State of the art surveys in Comp. Mechanics*, ASME, 1988.

[5] E. Priolo and G. Seriani, A numerical investigation of Chebyshev spectral element method for acoustic wave propagation, *Proc. of 13th IMACS World Congress on Comp. Applied Math.*, Dublin, **2** pp. 551–556, 1991.

[6] G. Seriani and E. Priolo, "High-order spectral element method for acoustic wave modeling", *61st SEG Annual Meeting Expanded Abstracts*, Houston, **2**, pp. 1561–1564, 1991.

[7] B. Fornberg, "The pseudospectral method: Accurate representation of interfaces in elastic wave calculations", *Geophys.* **53**, pp. 625–637, 1988.

[8] R.A. Renault and J. Petersen, "Stability of wide-angle absorbing boundary conditions for the wave equation", *Geophys.* **54**, 1153–1163, 1989.

[9] J. Tuomela, "Absorbing boundary conditions for the wave equations, curvature and finite elements", INRIA Rapports de Recherche 1513, 1991.

[10] T.J.R. Hughes, *The Finite Element Method*, Prentice Hall, Englewood cliffs, 1987.

[11] P. Berg, F. If, P. Nielsen and O. Skovgaard, "Diffraction by a wedge in an acoustic constant density medium", *Geophysical Prospecting* **41**, pp. 803–831, 1993.